



Anti-sway control of marine cranes under the disturbance of a parallel manipulator

Ayman A. Elbadawy · Mina M. G. Shehata

Received: 8 October 2014 / Accepted: 14 May 2015
© Springer Science+Business Media Dordrecht 2015

Abstract Cranes are used to move loads from one location to another in minimum time such that the load reaches its destination without swinging. This swinging problem gets aggravated in the presence of external disturbances such as in the case of marine cranes. This paper investigates the modeling of a tower crane model and different types of control schemes for both anti-swaying and input tracking control for the tower crane model under continuous external disturbances. The input shaping technique was applied for a tower crane model under continuous external disturbance. Then a closed-loop PID input shaper was implemented instead of the open-loop input shaper to compensate for the external disturbances. Also the response of the closed-loop PID input shaper was compared to a controller based on inverse dynamics. Environmental disturbances such as sea waves were simulated by the movement of a Stewart platform.

Keywords Stewart platform · Tower crane · Gantry crane · Input shaping · Anti-sway · Inverse dynamics · Nonlinear control

A. A. Elbadawy
Mechanical Engineering Department, Al-Azhar University,
Cairo, Egypt

A. A. Elbadawy (✉) · M. M. G. Shehata
Mechatronics Engineering Department, German University
in Cairo, Cairo, Egypt
e-mail: ayman.elbadawy@guc.edu.eg

1 Introduction

Cranes are used to move a load from point to point in minimum time such that the load reaches its destination without swinging. Usually a skillful operator is responsible for this task. During the operation, the load is free to swing in a pendulum-like motion. If the swing exceeds a proper limit, it must be damped or the operation must be stopped until the oscillations die out. It is practically impossible to completely remove payload oscillations in all possible circumstances. External disturbances such as wind can easily initiate an oscillation. Even without external disturbances, oscillations due to the movement of the tower crane are still hard to suppress.

This swinging problem gets aggravated in the presence of external disturbances such as in the case of marine cranes. According to the United States military logistics over shore department, marine cranes operations should be performed in sea state 0 through sea state 3. Conditions above sea state 3 occurs 15 % of the times [1]. Researchers have therefore tried to find different ways to control the movement of cranes in order to prevent and reduce the payload swinging.

Input shaping is an open-loop controller that drives the system to cancel out its own oscillations [2–6]. Input shaping is implemented in real time by convolving the command signal with an impulse sequence. Singer et al. [7] showed that input shaping could be robust to uncertainties in the system parameters using different configurations of input shapers. They demonstrated

that the four-pulses (ZVDD) input shaper is the most robust and most efficient input shaper algorithm of the input shapers algorithms mentioned previously. Blackburn et al. [8] also proved later on that the four-pulse input shaper is better than the radial- motion assisted command shapers for nonlinear tower crane rotational slewing. In their paper, they tried including the radial motion of trolley while rotating the jib of the tower crane in order to improve the efficiency of the input shaper and to reduce the sway angle. Other papers discussed adding PID controllers for input tracking with the input shapers [9–11]. Although all the previously mentioned efforts, the resulting open-loop controller is still sensitive to external disturbances and to parameter variations.

On the other hand, other researchers were studying the use of feedback control which is well known to be less sensitive to disturbances and parameter variations. Researchers started to study the underactuated mechanical systems [12,13]. Underactuated mechanical systems are systems with less number of control inputs than the degrees of freedom. Researchers discussed the use of PD controller to control the inverted pendulum [14]. Aguilar-Avelar et al. [15,16] presented a nonlinear controller using feedback linearization to control the Furuta pendulum.

Other researchers also adopted the feedback control for controlling the gantry crane system. Sorensen et al. [17] have presented a feedback PID control in addition to the input shaper to control both the position and the sway angle. They applied their controller on a simple one-dimensional gantry crane. Their control algorithms included a closed-loop PID input shaper. In order to test their external disturbances rejection module, they applied a single, non-continuous, impulse disturbance to the payload of the gantry crane. Some researchers proposed using delayed feedback controllers for both the position and the anti-swing controls proposed using delayed feedback controllers [18,19]. Furthermore, some researchers tried applying a controller based on fuzzy logic [20,21]. The proposed fuzzy logic controllers consist of position as well as anti-sway controllers.

Most of the previously mentioned work was done on a one-dimensional, one degree-of-freedom gantry crane. Also most of the previously mentioned work did not include continuous external disturbance, but rather a single-impulse external disturbance. This work studies the case of a two degree-of-freedom tower crane

model under continuous external disturbance. To simulate this case, the tower crane model was mounted on top of a Stewart platform. The movement of the Stewart platform will simulate the external disturbances such as the sea waves. Stewart platform is one of the most popular parallel manipulators. It has six degree-of-freedom positioning system that consists of two bodies connected by six legs. The Stewart platform was originally proposed and presented in 1965 as a flight simulator [22].

This paper presents the development of control algorithms for both the input tracking and anti-swaying of a tower crane model system under continuous external disturbances. The controller consists of a feedback PID control in addition to a closed-loop input shaper to control both the position and the sway angle. For the tower crane model, the sway angle is composed of a radial direction swing angle due to the movement of the trolley and a tangential direction swing angle due to the rotation of the jib. Then a controller based on the inverse dynamics of the tower crane model is put into comparison with the closed-loop PID input shaper. Numerical simulations were compared with the experimental setup. The performance of the control schemes is examined in terms of sway angle reduction.

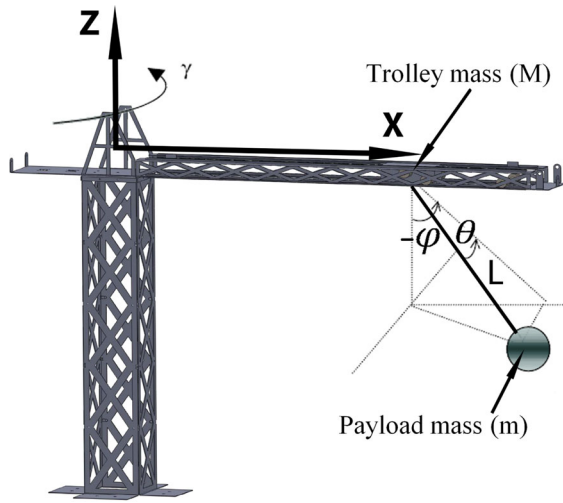
2 Dynamic modeling

To derive the equations of motion of the tower crane, the coordinate system has to be clearly defined. The cartesian coordinate system (xyz) is centered at a reference point that lies in the plane of the jib at the center of the crane tower, with its positive z -axis being along the tower upward axis (Fig. 1).

The x -axis and the y -axis are in the plane of the jib, with the x -axis being along the jib. The xyz coordinate system is attached to the rotating jib. The jib rotates and traces an angle $\gamma(t)$. The trolley moves on the jib with its position $r(t)$ being the distance measured from the origin of the xyz coordinate system. The angle $\gamma(t)$ and the radial distance $r(t)$ are the inputs to the system. They are used to control the system behavior.

2.1 Modeling of tower crane

Lagrangian approach was used to derive the equations of motion of the tower crane [18,19,23–29]. The vector \vec{r}_L defining the payload position is given by

**Fig. 1** Tower crane model

$$\vec{r}_L = \{x - L \cos(\theta) \sin(\varphi), L \sin(\theta), -L \cos(\theta) \cos(\varphi)\} \quad (1)$$

where

x defines the cart position in the x -direction, φ is the swing angle in the radial direction, in plane of the jib, due to the displacement of the tower crane's trolley and θ is the swing angle in the tangential direction due to the rotation of the tower crane's jib.

The vector \vec{r}_T defining the trolley position is given by

$$\vec{r}_T = \{x, 0, 0\} \quad (2)$$

The angular velocity of the tower crane ω is given by

$$\vec{\omega} = \{0, 0, \dot{\gamma}\} \quad (3)$$

The velocities of the trolley and the payload can be calculated using

$$\dot{r}(t) = \frac{dr(t)}{dt} + \vec{\omega} \times r(t) \quad (4)$$

The kinetic energy (T) is given by

$$T = \frac{1}{2}m_{\text{load}}(\dot{r}_L \cdot \dot{r}_L) + \frac{1}{2}M(\dot{r}_T \cdot \dot{r}_T) + \frac{1}{2}J_0\dot{\gamma}(t)^2 \quad (5)$$

Potential energy (V) is given by

$$V = -m_{\text{load}}g L \cos(\theta) \cos(\varphi) \quad (6)$$

Where the generalized displacement vector

$$\vec{q} = \{x, \varphi, \gamma, \theta\} \quad (7)$$

and the corresponding generalized force vector \vec{F}

$$\vec{F} = \{F_x, 0, T_\gamma, 0\} \quad (8)$$

Implementing Lagrange's equations, assuming small swing angles and neglecting the cable length variations yield to the following four nonlinear coupled equations

$$M\ddot{x} + m\ddot{x} + ml\varphi\dot{\varphi}^2 - ml\ddot{\varphi} = F_x \quad (9)$$

$$\ddot{\varphi} = -\frac{g}{L}\varphi + \frac{1}{L}\ddot{x} \quad (10)$$

$$(J_o + (M+m)x^2)\ddot{\gamma} + mlx(-\theta\dot{\theta}^2 + \ddot{\theta}) = T_\gamma \quad (11)$$

$$\ddot{\theta} = -\frac{g}{L}\theta - \frac{x}{L}\ddot{\gamma} \quad (12)$$

As shown from the equations, the system inputs are F_x and T_γ . Reformulating the equations in terms of motors input voltages, the two motors are modeled as constant gains

$$F_x = K_{mx}V_x \quad (13)$$

$$T_\gamma = K_{m\gamma}V_\gamma \quad (14)$$

where

K_{mx} is the tower crane's trolley motor constant gain, V_x is the input voltage for the tower crane's cart motor, $K_{m\gamma}$ is the tower crane's jib motor constant gain and V_γ is the input voltage for the tower crane's jib motor.

The DC motors transfer functions relating the displacement of the trolley with the input voltage V_x and the jib's rotation with the input voltage V_γ .

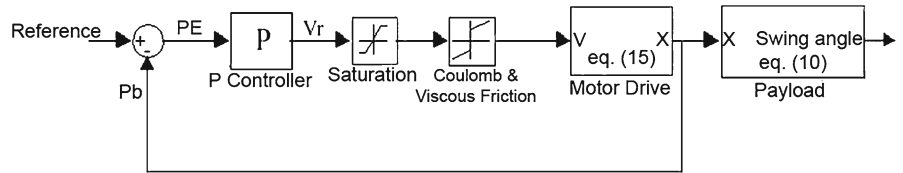
$$\frac{x(s)}{V_x(s)} = \frac{K_{tx}K_{trx}}{s[(L_{\text{ind}x}s + R_{\text{coil}x})(J_{mx}s + B_{mx}) + K_{bx}K_{tx}]} \quad (15)$$

$$\frac{\gamma(s)}{V_\gamma(s)} = \frac{K_{t\gamma}K_{tr\gamma}}{s[(L_{\text{ind}\gamma}s + R_{\text{coil}\gamma})(J_{m\gamma}s + B_{m\gamma}) + K_{b\gamma}K_{t\gamma}]} \quad (16)$$

where

K_t is the motor's torque constant gain, K_{tr} is the transmission ratio constant gain relating the motors rotations to the trolley displacement, and the jib rotation, L_{ind} is the inductance of the motor, R_{coil} is the resistance of the motor, J_m is the load inertia including both the motor's rotor inertia and the load inertia, B_m is the damping factor and K_b is the back emf constant gain.

Fig. 2 No swing control block diagram



2.2 Numerical simulations

The previously derived equations of motion were implemented and numerically simulated using Simulink. The block diagram of the system with no swing control is shown in Fig. 2. There is a feedback signal for the positioning module, while there is no feedback on the swing angle controller. The tower crane model is composed of two sub-systems: the trolley displacement and the jib rotation. For convenience purposes, all the block diagrams in this paper represent only the trolley sub-system. As for the jib sub-system, Eqs. (9, 10, 13), and (15) will be replaced by Eqs. (11, 12, 14), and (16), respectively. A desired reference position is issued to the controller. The reference signal and the feedback signal, P_b , are compared together to generate an error signal PE . The error signal is then sent to the P controller that generates an output signal corresponding to the desired output voltage, V_r . The output voltage goes through a saturation block to prevent the signal from going over the voltage limit of the motors.

The above derived mathematical model of the tower crane does not include any friction model. Friction is an unavoidable effect in mechanical system, and it may seriously degrade the performance of control systems. The problem is significant when high precision positioning is required. Friction characteristic is highly non-linear and may also vary with time. In addition, identification of the friction characteristic is a complex task [30]. The friction force reaches its peak value, μ_s , at very low speed, $v \approx 0$. The friction of the system was represented in the system block diagram by the coulomb and viscous friction block. The value of μ_s was identified experimentally and then used in the simulations.

Substituting with the input voltage in Eq. (15), the displacement of the trolley or the rotation of the jib could be calculated. Given the displacement of the system, the swing angle could be calculated from Eq. (10). The system was given an input of 25-cm displacement for the trolley and 20 degrees for the rotation of the jib. Figures 3, 4, 5, 6, 7, and 8 show the response of

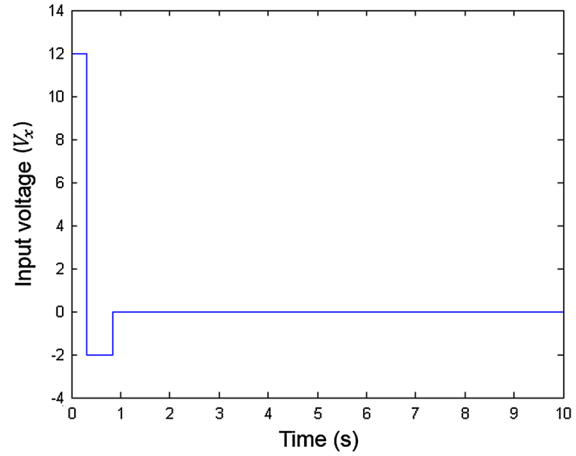


Fig. 3 Simulation response of the input voltage to the trolley's motor with no swing control

the system with no swing control, which is similar to a human operator. The figures show that there are no steady-state errors in the positioning of both the trolley and the jib, but the responses of the payload show high oscillation values. The value of the oscillations reached 0.31 rad in the radial direction and a value of 0.18 rad in the tangential direction. Both the radial and the tangential swinging had an oscillating frequency of 0.7 Hz because the length of the rope used in both the simulation and the experimental setup was 0.5 m.

In this work, the tower crane model is under continuous disturbance, similar to the case of marine cranes. To model such situation, the tower crane was mounted on top of a Stewart platform. The movement of the Stewart platform simulates the external disturbances, Fig. 9.

2.3 Modeling of stewart platform

The Stewart platform is shown in Fig. 10. The lower body is called the base and the upper is called the platform [31–33]. Each of the six legs has one of its endpoints fixed in the base and the other end point fixed in the platform. These legs are linear actuators that can

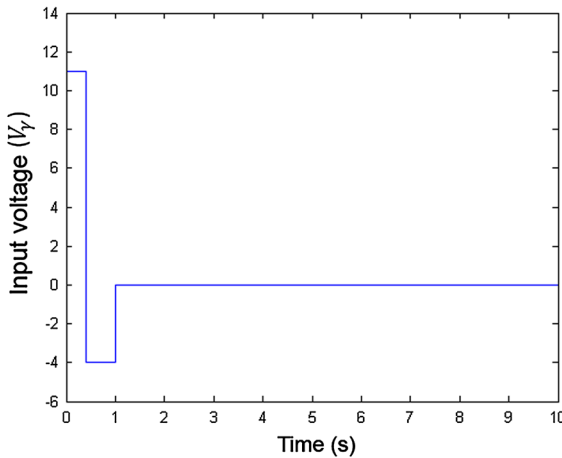


Fig. 4 Simulation response of the input voltage to the jib's motor with no swing control

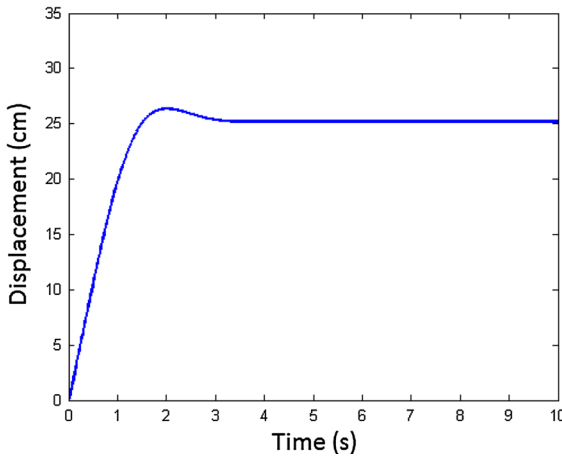


Fig. 5 Simulation response of the trolley displacement with no swing control

vary in length and each leg is considered to be composed of two different bodies connected by a prismatic joint.

For a given input disturbance to the tower crane model, the motion of the upper platform of the Stewart platform has to be known in terms of the three translational positions (x_{sp} , y_{sp} , z_{sp}) and the three rotational angles (θ_{xsp} , θ_{ysp} , θ_{zsp}). The objective of the Stewart platform's inverse kinematics is to determine the length of each individual leg to achieve the required position and orientation. It is also important to notice that the Stewart platform does not have independent drive systems for each degree of freedom, but rather achieves motion in all degrees of freedom by a combi-

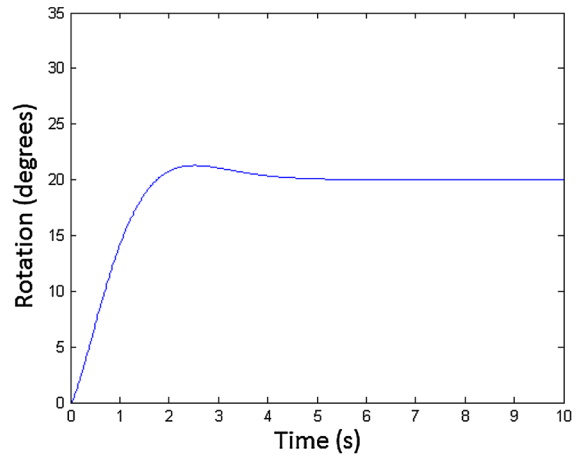


Fig. 6 Simulation response of the jib rotation with no swing control

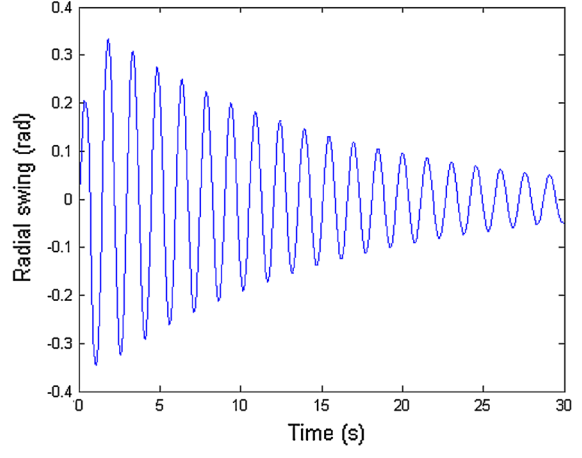


Fig. 7 Simulation response of the radial swing angle with no swing control

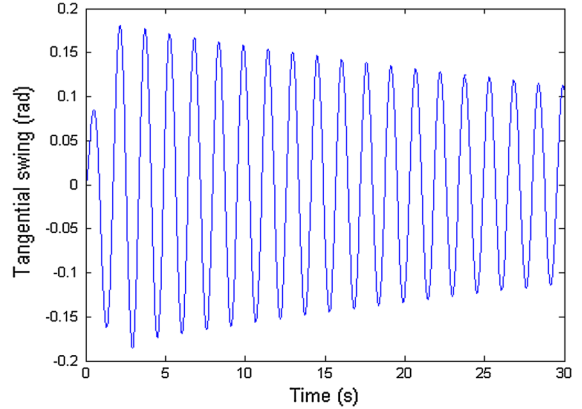


Fig. 8 Simulation response of the tangential swing angle with no swing control



Fig. 9 Tower crane mounted of a Stewart Platform

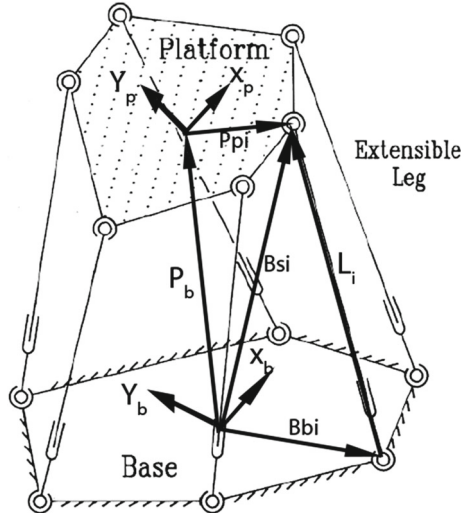


Fig. 10 Stewart Platform

nation of all actuator extensions. Since the Stewart platform consists of two bodies, it is convenient to define two coordinate systems, $[X_b, Y_b, Z_b]$ for the lower base and $[X_p, Y_p, Z_p]$ for the upper plate. The first coordinate system will be the global reference frame that is attached to the centroid of the base since the base is always grounded and do not move. The second coordinate system is attached to the centroid of the moving platform.

A transformation matrix will be used to transform vectors from platform coordinates to base coordinates.

The transformation matrix =

$$R = R_{zyx} = R_p^b = R_z(\theta_{zsp}) \times R_y(\theta_{ysp}) \times R_x(\theta_{xsp}) \quad (17)$$

where $R_z(\theta_{zsp})$, $R_y(\theta_{ysp})$, $R_x(\theta_{xsp})$ are the rotational matrices around the z -axis, y -axis and z -axis respectively.

$$P_b = [x, y, z + \text{offset}] \quad (18)$$

$$B_{si} = P_b + (R_p^b \times P_{pi})_b \quad (19)$$

$$B_{bi} = B_{si} - L_i \quad (20)$$

$$L_i = B_{si} - B_{bi} \quad (21)$$

$$L_i = P_b + (R_p^b \times P_{pi})_b - B_{bi} \quad (22)$$

The required length of each leg is equal to the magnitude of the vector L_i , where $i=1,\dots,6$

In order to determine the effect of the movement of the Stewart platform on the payload of the tower crane, it is required to define a transformation matrix between the Stewart platform's upper plate and the trolley position.

Defining $\vec{r}_{T/P}$ which is the position of the tower crane's trolley in the x -direction, y -direction and z -direction respectively with respect to the coordinate system $[X_p, Y_p, Z_p]$. The new position of the trolley after the movement of the Stewart platform is given by

$$\vec{r}_{T/P2} = \begin{bmatrix} R_{zyx} & S_{tr} \\ 0 & 1 \end{bmatrix} \begin{bmatrix} \vec{r}_{T/P} \\ 1 \end{bmatrix} = [x_2, y_2, z_2, 1] \quad (23)$$

$$S_{tr} = [x_{sp}, y_{sp}, z_{sp}] \quad (24)$$

where,

S_{tr} is a vector containing the translational motions of the Stewart platform.

Numerically integrating Eqs. (9–12), the radial swing angle is calculated by substituting the variable x by x_2 in (9) and (10), and the tangential swing is calculated by substituting γ by $(\gamma + \theta_{zsp})$ in (11) and (12).

Figures 11 and 12 show the simulations of the system when given an input of 25-cm displacement for the trolley and 20° for the rotation of the jib under continuous external disturbance. The external disturbance was caused by the movement of the Stewart platform. The Stewart platform was actuated to rotate sinusoidally around both the x -axis and the z -axis with an amplitude of 4° and 8° respectively and with a frequency of 3 Hz. The value of the oscillations is higher compared to

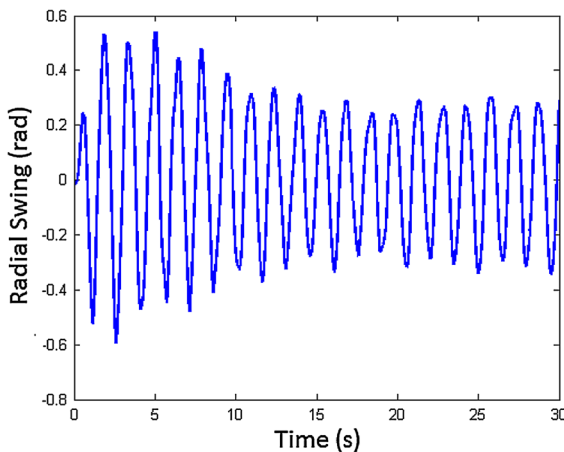


Fig. 11 Simulation response of the radial swing angle with no swing control under continuous external disturbance

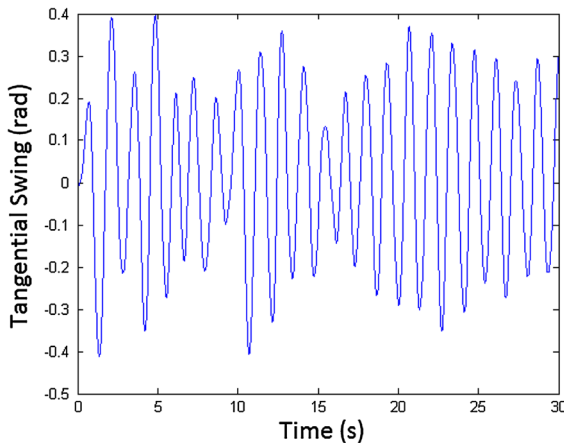


Fig. 12 Simulation response of the tangential swing angle with no swing control under continuous external disturbance

the previous simulation with no external disturbance. The value of the oscillations reached 0.59 rad in the radial direction and a value of 0.4 rad in the tangential direction.

3 Control schemes

3.1 Open-loop input shaper

The input shaping is an open-loop control method that is going to be used to guarantee free vibration of cargo of the tower crane. It is a successful approach to suppressing oscillations by generating a reference command that drives the system to cancel out its own oscillations. Input shaping is implemented by convolving a

sequence of impulses, known as input shaper, with a reference signal [34–39]. The shaped command is then used to drive the system.

The amplitudes and time locations of the impulses comprising the input shaper are determined by solving a set of constraint equations that attempt to limit the unwanted system dynamics. In this work, the ZVDD input shaper was used because it is more effective than the other input shaper techniques and it is more robust for the system parameters variations up to $\pm 40\%$. The ZVDD input shaper is defined by four impulses, where their sum must be equal to a unity magnitude. The four impulses and their corresponding time are defined by

$$t_1 = 0, t_2 = 0.5T_D, t_3 = T_D, t_4 = 1.5T_D \quad (25)$$

$$A_1 = \frac{1}{D}, A_2 = \frac{3K}{D}, A_3 = \frac{3K^2}{D}, A_4 = \frac{K^3}{D}$$

where

$$D = 1 + 3K + 3K^2 + K^3, \quad K = e^{\frac{-\xi\pi}{\sqrt{1-\xi^2}}} \\ T_D = \frac{2\pi}{\omega_d} = \frac{2\pi}{\omega_o\sqrt{1-\xi^2}}, \quad \omega_o = \sqrt{\frac{g}{L}}$$

The block diagram of the open-loop input shaper controller is shown in Fig. 13. A desired reference position is issued to the controller. The reference position is sent to the input shaper to determine the impulses magnitudes and time of their occurrences.

The shaped reference signal and the feedback signal, P_b , are compared together to generate an error signal PE . The error signal is then sent to the PID controller that generates an output signal corresponding to the desired output signal, V_r . The output signal goes through a saturation block to prevent the signal from going over the voltage limit of the motors. The saturated control signal then goes through the coulomb and viscous friction to compensate for the system friction. Substituting with the input voltage in Eq. (15) or (16), the displacement of the trolley or the rotation of the jib could be calculated. Given the displacement of the system, the swing angle could be calculated from Eq. (10) or (12).

For the input shaping controller, only Eqs. (10) and (12) are utilized, the rest of the system dynamics and parameters are not taken into consideration. The open-loop input shaping controller was simulated under the same conditions as before by giving it an input of 25-cm displacement for the trolley and 20° for the rotation of the jib. Figures 14, 15, 16, 17, 18, and 19 show the response of the system using the open-loop input

Fig. 13 Open-loop input shaper block diagram

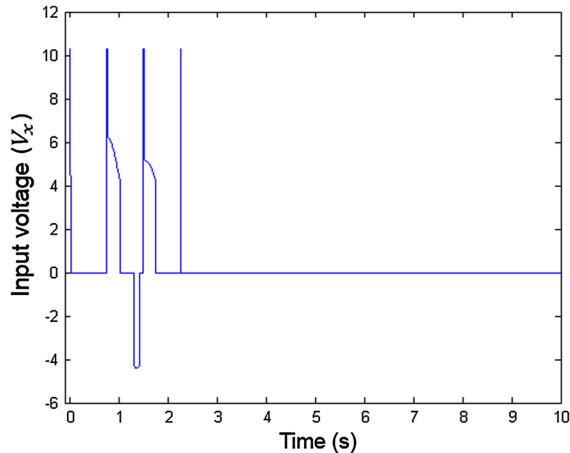
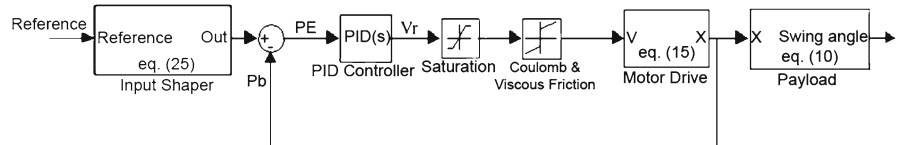


Fig. 14 Simulation response of the input voltage to the trolley's motor with open-loop input shaping

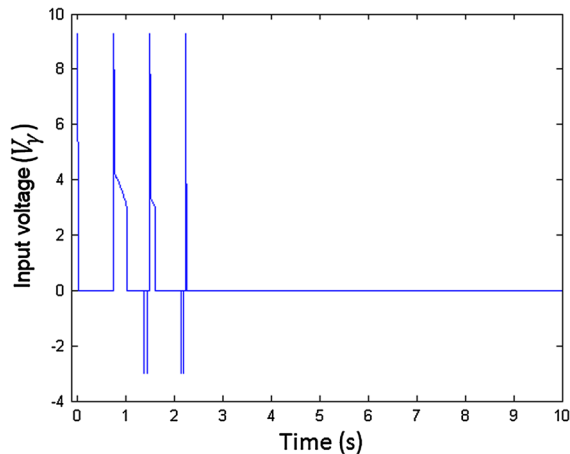


Fig. 15 Simulation response of the input voltage to the jib's motor with open-loop input shaping

shaper algorithm. It is shown that the swing angle has been reduced in both the radial and tangential directions compared to the previous simulations when there was no swing control. The figures show that there are no steady-state errors in the positioning of both the trolley and the jib, and the responses of the payload show small oscillations values. The value of the oscillations reached 0.14 rad in the radial direction and a value of 0.07 rad in the tangential direction.

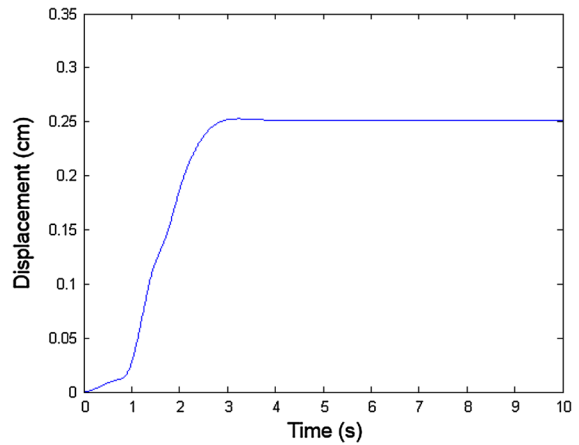


Fig. 16 Simulation response of the trolley displacement with open-loop input shaping

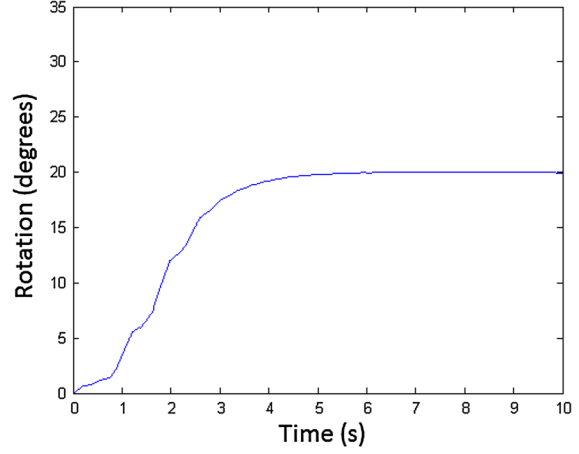


Fig. 17 Simulation response of the jib rotation with open-loop input shaping

The previously mentioned controller does not incorporate a feedback for the swing angles, which makes the controller unresponsive to external disturbances. The open-loop input shaper was tested in the presence of external disturbances from the Stewart platform. The Stewart platform was actuated to rotate sinusoidally around both the x -axis and the z -axis with an amplitude of 4° and 8° respectively and with a frequency of 3 Hz. Figures 20 and 21 show the response of the

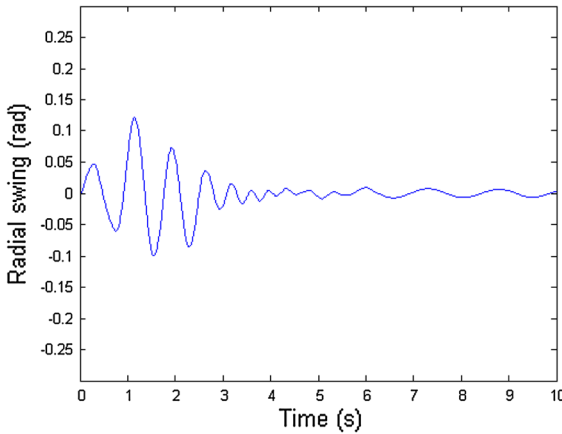


Fig. 18 Simulation response of the radial swing angle with open-loop input shaping

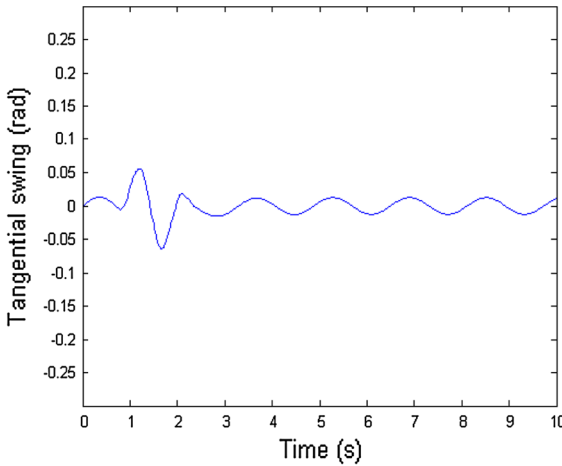


Fig. 19 Simulation response of the tangential swing angle with open-loop input shaping

payload with the open-loop input shaper when given the same inputs of 25 cm and 20° but under continuous external disturbance from the Stewart platform. It is clearly shown that the controller was no longer able to suppress the oscillations. The value of the oscillations reached 0.32 rad in the radial direction and a value of 0.35 rad in the tangential direction.

3.2 Closed-loop PID input shaper

In order for the input shaper controller to be responsive to external disturbances, a closed-loop PID input shaper controller was implemented. The closed-loop PID input shaper block diagram is shown in Fig. 22

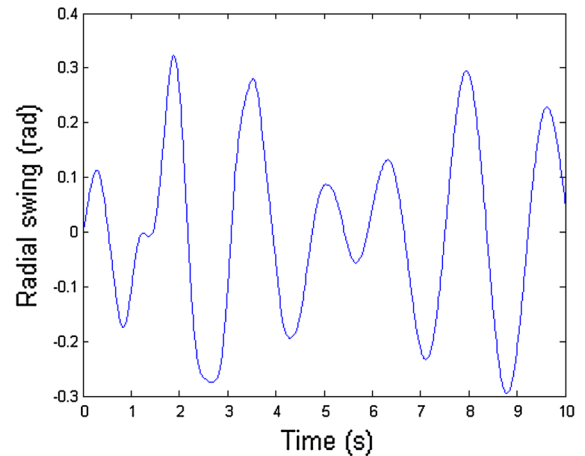


Fig. 20 Simulation response of the radial swing angle with open-loop input shaping under continuous external disturbance

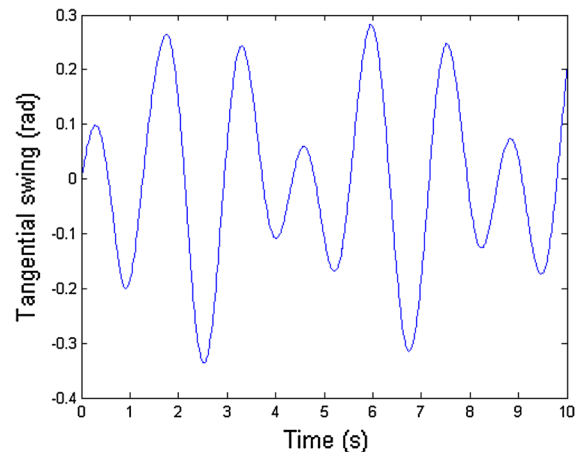


Fig. 21 Simulation response of the tangential swing angle with open-loop input shaping under continuous external disturbance

[17]. The control module was designed to eliminate the cable sway caused by external disturbances acting on the payload due to the movement of the Stewart platform. The control module was designed to eliminate the cable sway caused by external disturbances acting on the payload due to the movement of the Stewart platform. This type of disturbance may be modeled as inducing a disruptive angle, θ_d , summed with the undisturbed angle, θ_p , to produce the actual cable angle of the system, θ_a . The input shaper approach is based on suppressing the oscillations in plants by generating a shaping technique to work correctly, and the controller should be able to clearly distinguish between the disruptive angle, θ_d , and the undisturbed angle, θ_p . The

PID controller should be responsible for damping out the disruptive angle, while the undisturbed angle will be canceled out by the shaped reference signal. To distinguish between the disruptive angle and the undisturbed angle, the actual angle, θ_a , will be compared with the angle expected from the equations of motion of the payload model, θ_m , Eqs. (10) and (12). The angle error, θ_e , is the result from subtracting θ_m from θ_a . It is clear that θ_m will be equal to θ_a in case where there is no external disturbances. The angle error will be utilized in a PID block to generate a control signal, V_c that will damp out the disruptive oscillations. V_r is the control signal from the positioning module of the input shaper. The corrective output voltage signals, V_c and V_r , will be summed up together to generate the final output control signal, V_s . To maintain a maximum voltage limit, a saturation block truncates excessive voltage prior to being sent to the drives of the motors. The saturated control signal then goes through the coulomb and viscous friction to compensate for the system friction. Substituting with the input voltage into Eq. (15), the displacement of the trolley or the rotation of the jib could be calculated. Given the displacement of the system, the swing angle could be calculated from Eq. (10).

Closed-loop input shaping technique was used instead of the normally used open-loop input shaping in order to increase the efficiency of the algorithm and decrease the sway angle. Input shaping is a controller that utilizes the simulation time to generate the impulses at specific times. Once all impulses have been generated, the input shaper will be of no use. The advantage of using the closed-loop input shaper is that the simulation time resets each time the trolley or the jib has moved. By resetting the time, the input shaper will shape the new signal to compensate for the new movements of the plants. The results of the closed-loop PID input shaper is shown in the section of the experimental results.

Although the experimental evaluation of the closed-loop PID input shaper showed good results in reducing the oscillations, better results could be achieved if the system dynamics are taken into consideration.

The next section studies and compares the results of the closed-loop input shaper with the inverse dynamics controller. The inverse dynamics controller takes into consideration all the system parameters, including the parameters that were neglected in the input shaping controller which are the mass of the payload, the mass of the trolley and the inertia of the jib.

3.3 Inverse dynamics

Any dynamics model could be rewritten in the matrix form

$$M_i(q)\ddot{q} + C_i(q, \dot{q})\dot{q} + G_i(q) = F_i \quad (26)$$

where

$M(q)$ is the inertia matrix, $C(q, \dot{q})$ denotes a Coriolis and centrifugal matrix, $G(q)$ is a matrix of gravity vector and F indicates a matrix of control forces. The subscript, i , is used to differentiate between the system of the trolley displacement and the system of the jib rotation.

Substituting Eq. (10) into (9) and (12) into (11)

$$M\ddot{x} + ml\varphi\dot{\varphi}^2 + mg\varphi = F_x \quad (27)$$

$$J_o\ddot{\gamma} + Mx^2\ddot{\gamma} - mlx\theta\dot{\theta}^2 - mxg\theta = T_\gamma \quad (28)$$

The tower crane is an underactuated system having 4° of freedom (trolley displacement, jib rotation, load radial swing angle and load tangential swing angle), while having only two actuators. The overall mathematical model can be separated into four auxiliary system dynamics. The actuated model corresponds to the active states $q_{11} = [x(t)]$ and $q_{21} = [\gamma(t)]$, while the un-actuated model is represented by $q_{12} = [\varphi(t)]$ and $q_{22} = [\theta(t)]$.

The above actuated dynamics can be rewritten in matrix form

$$\overline{M}_i(q)\ddot{q}_{i1} + \overline{C}_i(q, \dot{q})\dot{q}_{i2} + \overline{G}_i(q) = U_i \quad (29)$$

where

$$\overline{M}_1(q) = M, \quad \overline{M}_2(q) = J_o + Mx^2$$

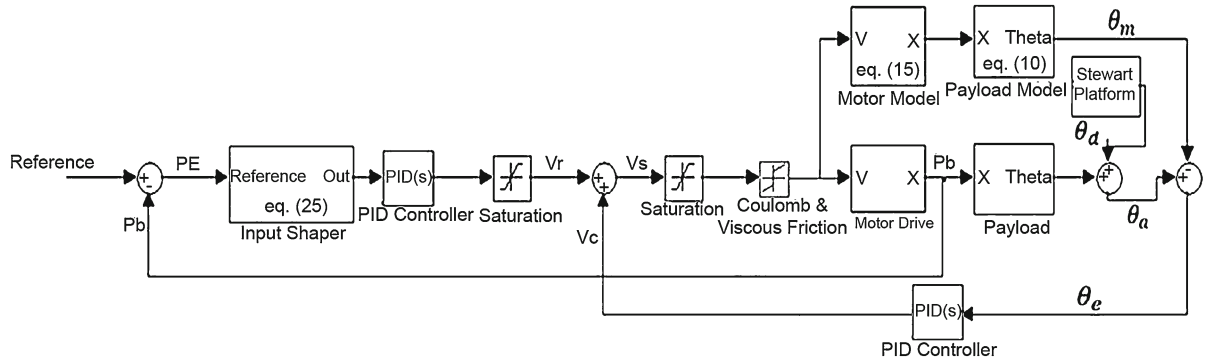
$$\overline{C}_1(q, \dot{q}) = mL\varphi\dot{\varphi}, \quad \overline{C}_2(q, \dot{q}) = -mlx\theta\dot{\theta}$$

$$\overline{G}_1(q) = mg\varphi, \quad \overline{G}_2(q) = -mxg\theta$$

The control signal U is utilized in the PID controller to generate a corresponding control signal that will drive the motors.

The actuated dynamics is represented by

$$\ddot{q}_{i1} = B_{ai}\dot{q}_{2i} + C_{ai} + D_{ai}U_i \quad (30)$$

**Fig. 22** Closed-loop PID input shaper block diagram

where

$$\begin{aligned} B_{ai} &= \frac{-\bar{C}(q, \dot{q})}{\bar{M}(q)} \\ C_{ai} &= \frac{-\bar{G}(q, \dot{q})}{\bar{M}(q)} \\ D_{ai} &= \frac{1}{\bar{M}(q)} \end{aligned}$$

To stabilize the actuated system dynamics, the equivalent control input should be chosen as

$$a_q = \ddot{q}_{i1} = \ddot{q}_{i1}^d - K_{di} (\dot{q}_{i1} - \dot{q}_{i1}^d) - K_{pi} (q_{i1} - q_{i1}^d) \quad (31)$$

where

K_{di} and K_{pi} are velocity and position gains respectively. The superscript, d , defines the required input state value.

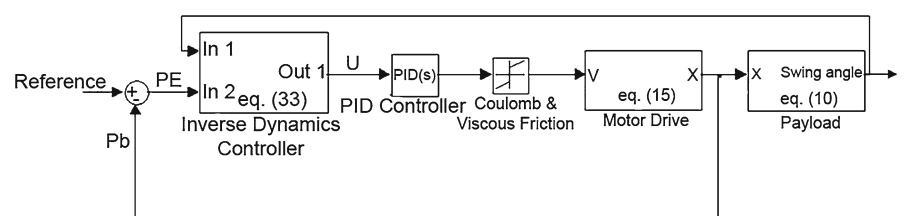
To guarantee the stability of both the actuated and un-actuated states, the nonlinear controller should include both states

$$\begin{aligned} a_q &= \ddot{q}_{i1} = \ddot{q}_{i1}^d - K_{di} (\dot{q}_{i1} - \dot{q}_{i1}^d) - K_{pi} (q_{i1} - q_{i1}^d) \\ &\quad + \ddot{q}_{i2}^d - K_{di} (\dot{q}_{i2} - \dot{q}_{i2}^d) - K_{pi} (q_{i2} - q_{i2}^d) \end{aligned} \quad (32)$$

The nonlinear control input signal is obtained by substituting Eqs. (30) and (32) [40, 41]

$$\begin{aligned} U_i &= -\bar{M}_i(q) (K_{di} \dot{q}_{i1} + (B_{ai} + K_{di}) \dot{q}_{i2} \\ &\quad + K_{pi} (q_{i1} - q_{i1}^d) + K_{pi} q_{i2} + C_{ai}) \end{aligned} \quad (33)$$

The block diagram of the above mentioned equation is shown in Fig. 23. The reference signal is then compared to the feedback signal, Pb , to generate an error signal PE. The error signal and the feedback angle signal are utilized in the inverse dynamics controller to generate a control signal U . The control signal U is then utilized in a PID controller to generate the corresponding required voltage. To maintain a maximum voltage limit, a saturation block truncates excessive voltage prior to being sent to the drives of the motors. The saturated control signal then goes through the coulomb and viscous friction to compensate for the system friction. Substituting with the input voltage in Eq. (15), the displacement of the trolley or the rotation of the jib could be calculated. Given the displacement of the system, the swing angle could be calculated from Eq. (10).

Fig. 23 Inverse Dynamics block diagram

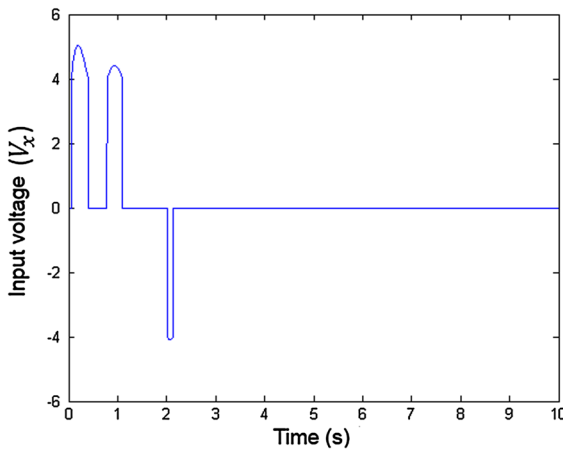


Fig. 24 Simulation response of the input voltage to the trolley's motor with inverse dynamics control

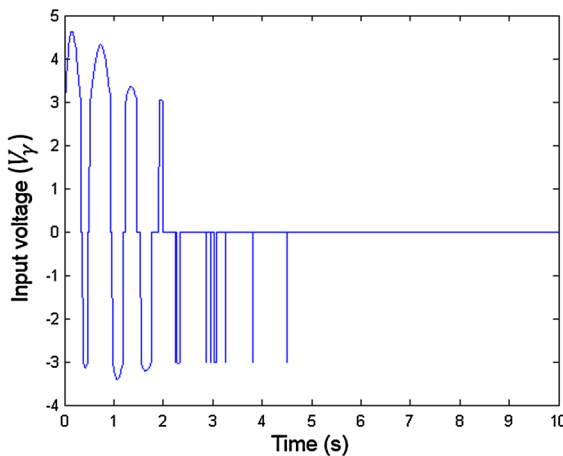


Fig. 25 Simulation response of the input voltage to the jib's motor with inverse dynamics control

In order to compare all the control schemes, the inverse dynamics controller was tested in the simulation environment under the same condition as before by giving it an input of 25-cm displacement for the trolley and 20° for the rotation of the jib. Figures 24, 25, 26, 27, 28, and 29 show the response of the payload using the inverse dynamics algorithm. The figures show small oscillations values in both the radial and tangential directions compared to the closed-loop input shaper simulations. The value of the oscillations reached 0.07 rad in the radial direction and a value of 0.03 radians in the tangential direction. Figures 30 and 31 show the response of the payload given the same inputs but under continuous disturbance using the inverse dynamics algorithm. The figures show that

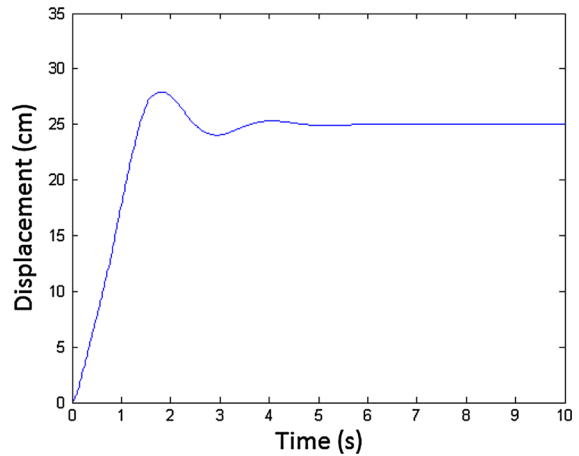


Fig. 26 Simulation response of the trolley displacement with inverse dynamics control

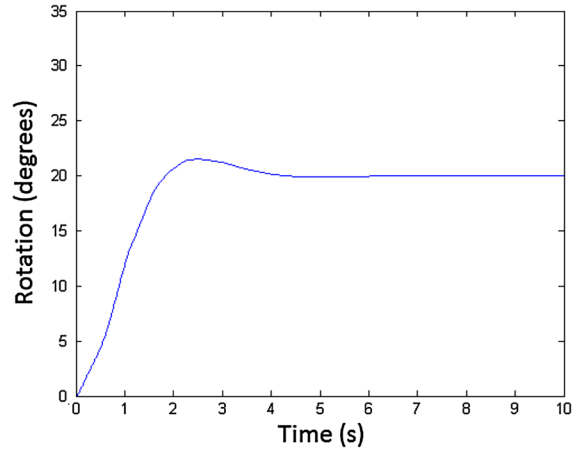


Fig. 27 Simulation response of the jib rotation with inverse dynamics control

the inverse dynamics reduces the oscillations in both the radial and the tangential directions. The value of the oscillations reached 0.07 rad in the radial direction and a value of 0.12 rad in the tangential direction.

4 Validation results

4.1 Experimental setup

The experimental hardware setup is shown in Fig. 32. The tower crane is mounted on top of the moving Stewart platform. The swinging of the payload was measured using a 9° of freedom inertial measurement unit "IMU." The IMU consists of a triple-axis gyroscope, a

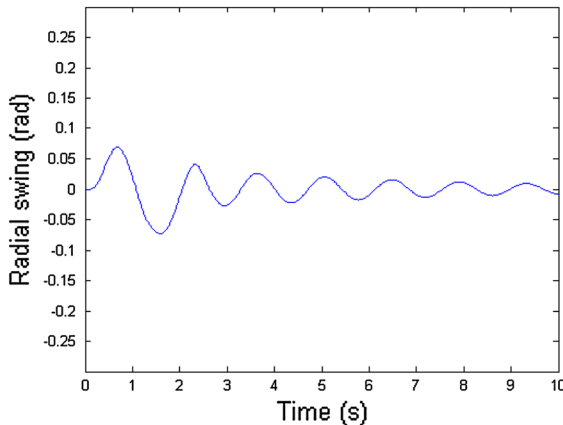


Fig. 28 Simulation response of the radial swing angle with inverse dynamics control

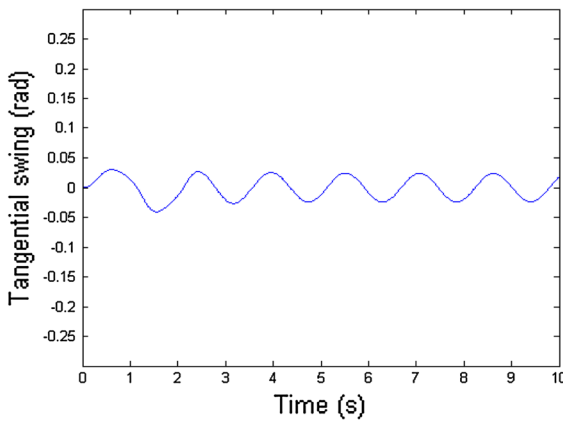


Fig. 29 Simulation response of the tangential swing angle with inverse dynamics control

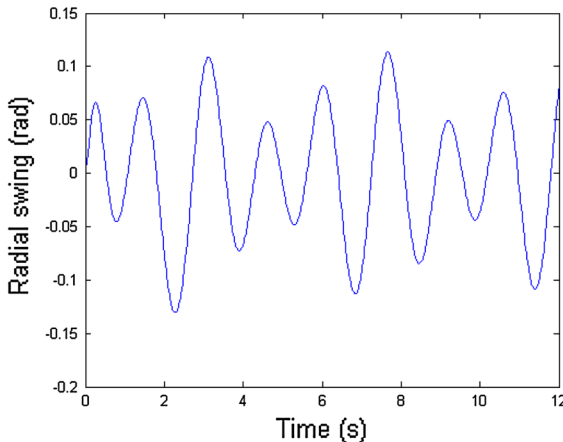


Fig. 30 Simulation response of the radial swing angle with inverse dynamics control under continuous external disturbance

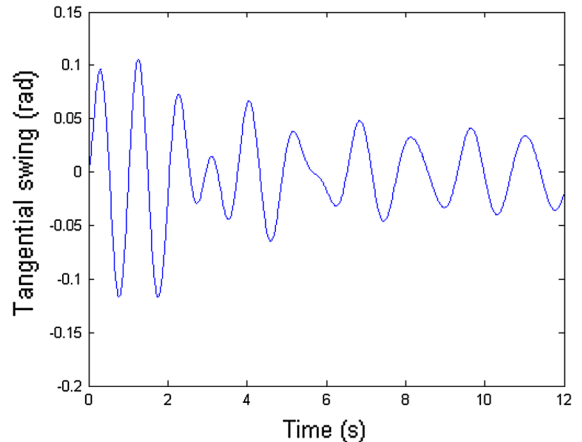


Fig. 31 Simulation response of the tangential swing angle with inverse dynamics control under continuous external disturbance

13-bit resolution accelerometer, and a triple-axis magnetometer. The pitch, roll, and yaw angles were calculated by a data fusion C++ library that makes use of the readings of all three sensors, in order to come up with a final output value with least error possible [42]. Also to make the readings as accurate as possible, all wirings have been removed and all the data from the IMU were transmitted to the PC wirelessly using a ZigBee module.

The hardware setup of the tower crane model was equipped with three brushed DC motors with built-in shaft encoders. One motor was responsible of the rotation of the tower crane's jib, one motor was used for the linear displacement of the cart, while the last motor was used for lifting and lowering of the payload. The tower crane motors are equipped with feedback encoders that provide pulses with the rotation of the motor's shaft. The hardware specifications are shown in Table 1. By counting the number of pulses, the feedback position of the trolley and the jib could be determined. The motors specifications are shown in Table 2. The unmeasurable values such as the motors damping and the payload damping factor are measured from experimental results. The motors load inertias are calculated for the 3D drawings of the experimental hardware setup. The friction constant, μ_s , was measured experimentally

$$\mu_s = 3.5$$

As for the Stewart platform, it was equipped with six linear actuators with built-in feedback. The feedback consists of a potentiometer mounted on the extensible

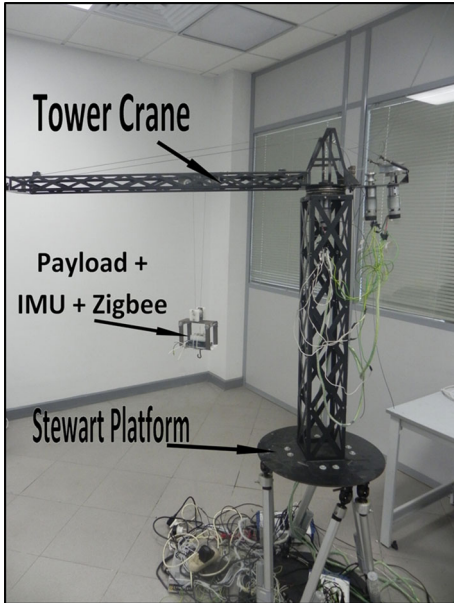


Fig. 32 Experimental setup hardware

Table 1 Experimental setup hardware specifications

Item	Specifications
Length of pendulum	0.5 m
Weight of pendulum	0.35 Kg
Weight of the cart	0.25 Kg
Jib rotation motor input voltage	12 V, 66 W
Cart displacement motor input voltage	12 V, 42 W
Jib rotation motor' encoder	840 ppr
Cart displacement motor' encoder	240 ppr

legs. The potentiometer returns a variable resistance which is proportional to the leg's length.

All of the control schemes were implemented on LabVIEW. LabVIEW is a parallel programming language which executes all the commands in a parallel way. The use of a parallel programming and multi-threading language was mandatory in order to control both the Stewart platform's actuators and the tower crane's actuators both at the same time. Also in order to properly control the movements of the Stewart platform, all of the legs should be actuated at the same time. The LabVIEW software is using a sampling rate of 1KHz. The controller calculates the required speed and position for each of the trolley and the jib depending

Table 2 Experimental setup motors specifications

Item	Specifications
Cart displacement motor specifications	$Speed = 248 \text{ rpm}$ $K_{tx} = 0.2 \text{ Nm/Amp}$ $K_{trx} = 0.0019$ $L_{indx} = 0.01 \text{ F}$ $R_{coilx} = 2\Omega$ $J_{mx} = 0.0006 \text{ Kg m}^2$ $B_{mx} = 0.00093 \text{ N s/m}$ $K_{bx} = 0.01 \text{ V/rpm}$
Jib rotation motor specifications	$Speed = 76 \text{ rpm}$ $K_{ty} = 0.4 \text{ Nm/Amp}$ $K_{try} = 0.0119$ $L_{indy} = 0.01 \text{ F}$ $R_{coily} = 2\Omega$ $J_{my} = 0.01 \text{ Kg m}^2$ $B_{my} = 0.013 \text{ N s/m}$ $K_{by} = 0.0029 \text{ V/rpm}$

on their current positions which is given by the encoders [$x(t)$ and $\gamma(t)$], and also depending on the current orientation of the payload which is calculated from the IMU data [$\varphi(t)$ and $\theta(t)$]. The speed of the motors was controlled using H-bridge circuits that send a PWM signal to the DC motors. The motors speed depends on the duty cycle of the PWM signal.

The interfacing between the controller and the H-bridge circuits was done using the NI-6251 data acquisition card. The NI 6251 is a USB high-speed multi-function DAQ device optimized for superior accuracy at fast sampling rates [43].

4.2 Implementation and results

In this section, the proposed control schemes are implemented and tested with the simulation environment. The control schemes were also implemented of the hardware setup, and both results were compared. The cart of the tower crane was required to move a total distance of 25 cm while the jib of the tower crane was required to rotate a total angle of 20°. Figures 33, 34, 35, 36, 37, 38, 39 and 40 show the responses of the tower crane's cart and the payload given the step input of 25 cm and 20° using the control schemes discussed earlier.

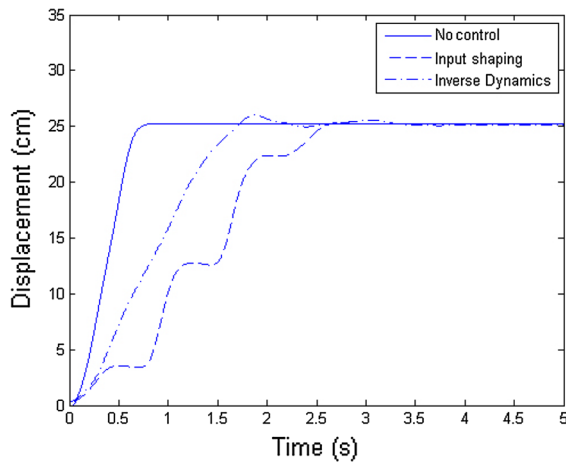


Fig. 33 Tower crane trolley response

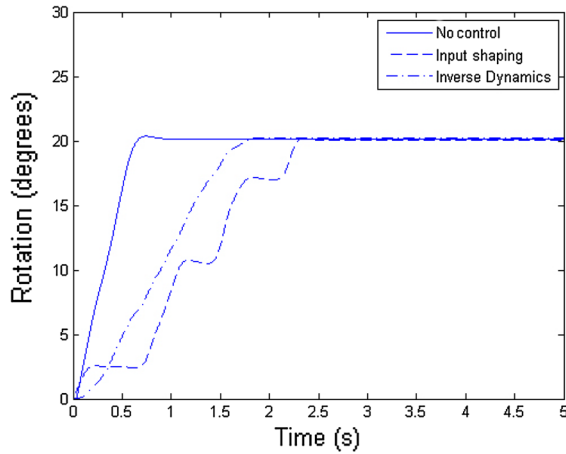


Fig. 34 Tower crane jib response

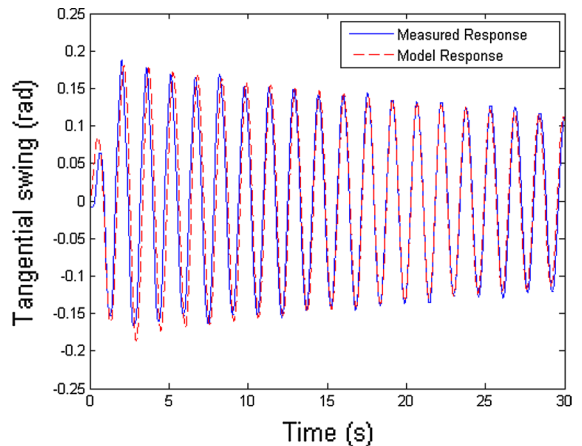


Fig. 36 Tangential swing with no swing control

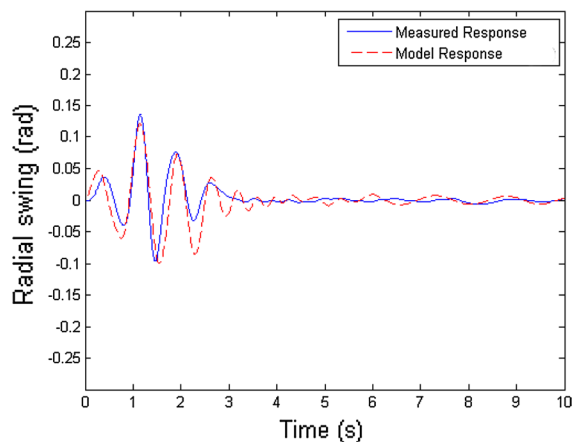


Fig. 37 Radial swing with input shaping

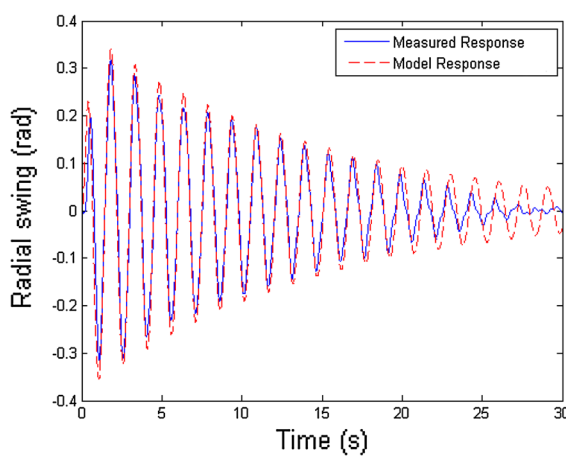


Fig. 35 Radial swing with no swing control

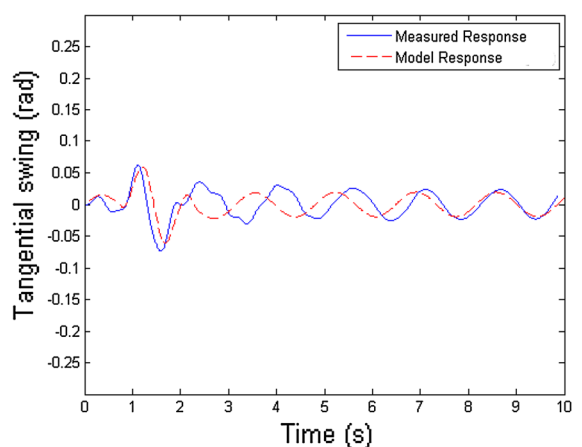
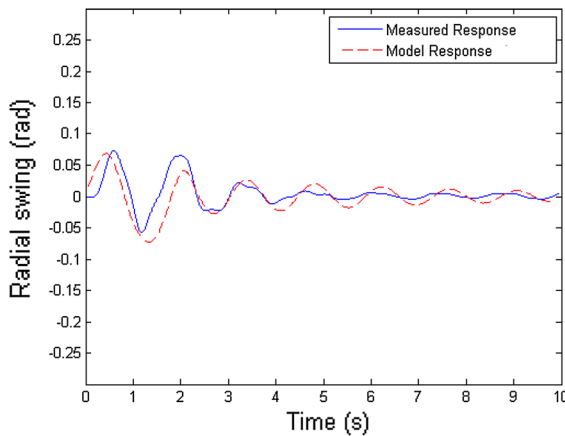
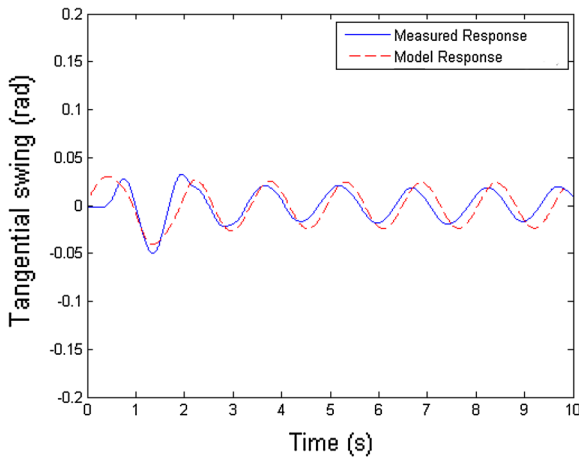
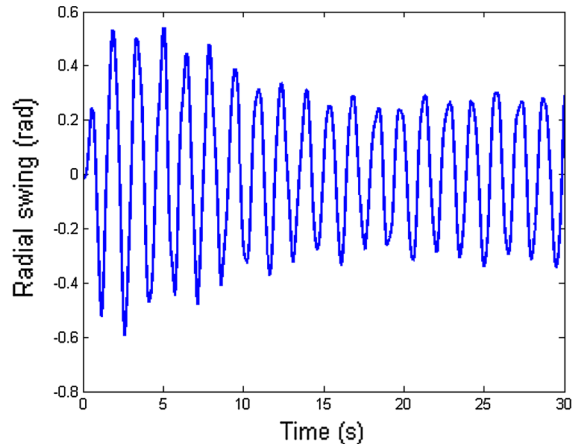
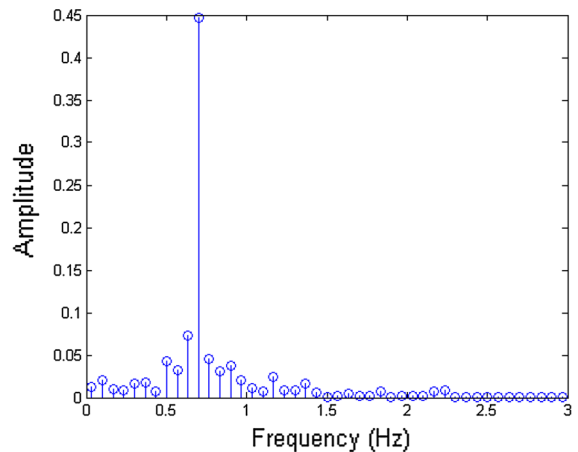
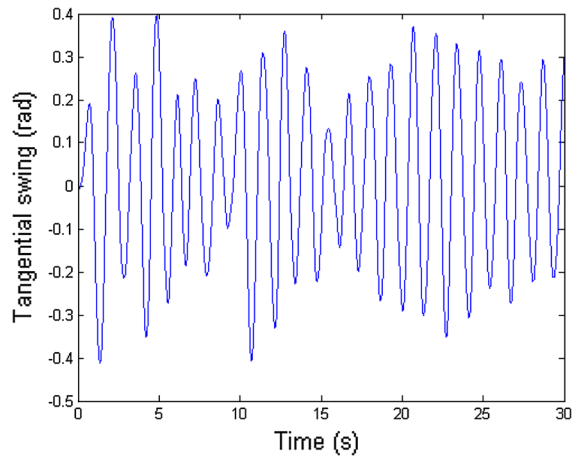


Fig. 38 Tangential swing with input shaping

**Fig. 39** Radial swing with inverse dynamics**Fig. 40** Tangential swing with inverse dynamics

The following figures show the response of the payload when the Stewart platform adds a continuous external disturbance to the tower crane. The Stewart platform was actuated to rotate sinusoidally around both the x -axis and the z -axis with an amplitude of 4° and 8° , respectively, and with a frequency of 3 Hz. The Stewart platform was chosen to rotate around both the x -axis and z -axis at the same time to cause a non-uniform disturbance for the tower crane to affect both swinging angles the radial and the tangential. The load in the tower crane was suspended from a rope having a length of 0.5 m, which results in a natural frequency of 0.7 Hz. The swing angles with no control were very high (Figs. 41, 42, 43, 44). The value of the oscillations reached 0.59 rad in the radial direction and a value of 0.4 rad in the tangential direction.

**Fig. 41** Radial swing with no swing control under continuous external disturbance**Fig. 42** Frequency spectrum of radial swing with no control under continuous external disturbance**Fig. 43** Tangential swing with no control under continuous external disturbance

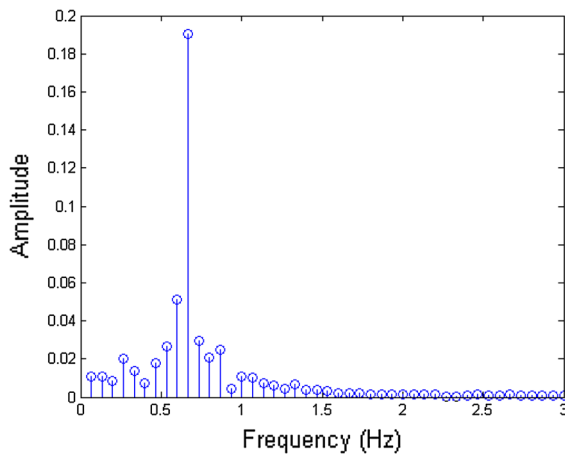


Fig. 44 Frequency spectrum of tangential swing with no control under continuous external disturbance

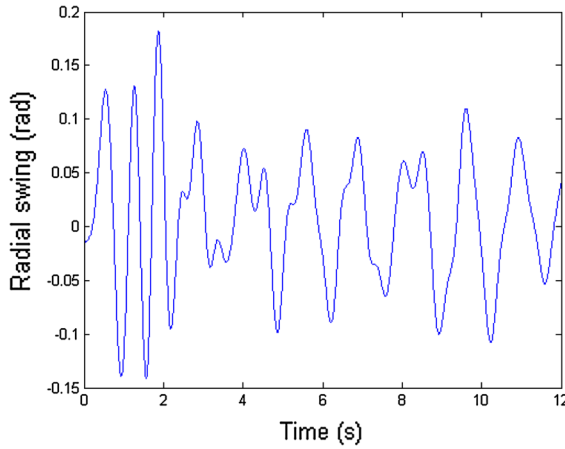


Fig. 45 Radial swing with input shaping under continuous external disturbance

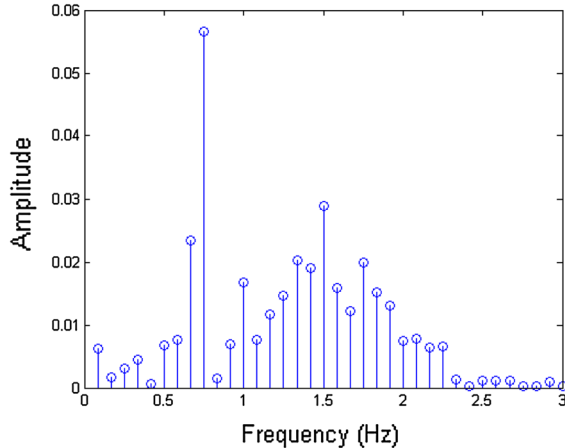


Fig. 46 Frequency spectrum of radial swing with input shaping control under continuous external disturbance

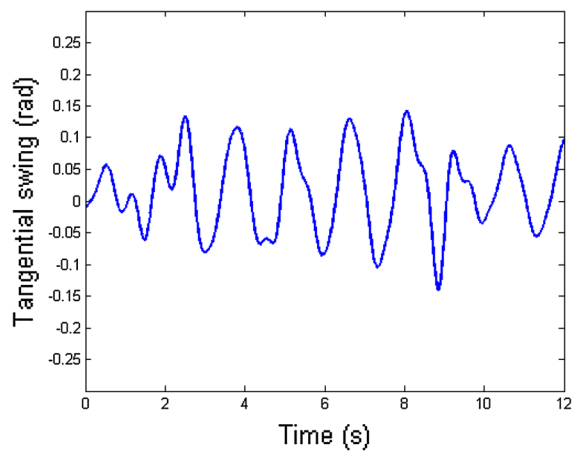


Fig. 47 Tangential swing with input shaping under continuous external disturbance

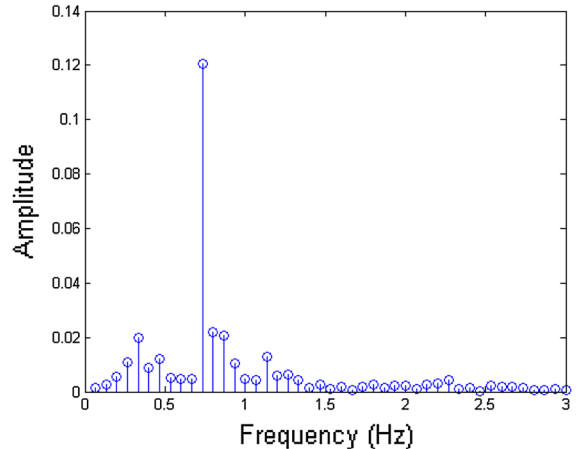


Fig. 48 Frequency spectrum of tangential swing with input shaping control under continuous external disturbance

The closed-loop input shaper was able to reduce the oscillations in the presence of external disturbance (Figs. 45, 46, 47, 48). As shown in the frequency spectrum figures, a frequency with double the natural frequency of the pendulum appeared that might be due to the parametric excitation imparted upon the payload due to the movement of the Stewart platform. The value of the oscillations reached 0.18 rad in the radial direction and a value of 0.14 rad in the tangential direction.

As shown in Figs. (49, 50, 51, 52), the inverse dynamics controller was the most effective controller in terms of rise time and sway angle suppression. The value of the oscillations reached 0.12 rad in the radial direction and a value of 0.13 rad in the tangential direction.

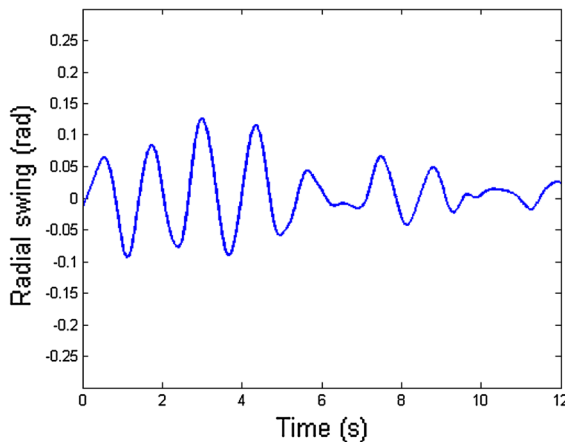


Fig. 49 Radial swing with inverse dynamics under continuous external disturbance

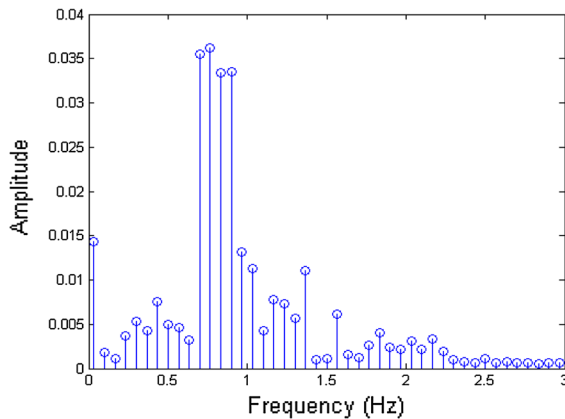


Fig. 50 Frequency spectrum of radial swing with inverse dynamics control under continuous external disturbance

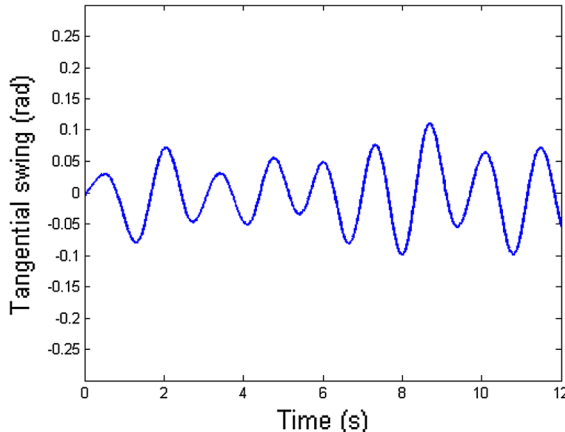


Fig. 51 Tangential swing with inverse dynamics under continuous external disturbance

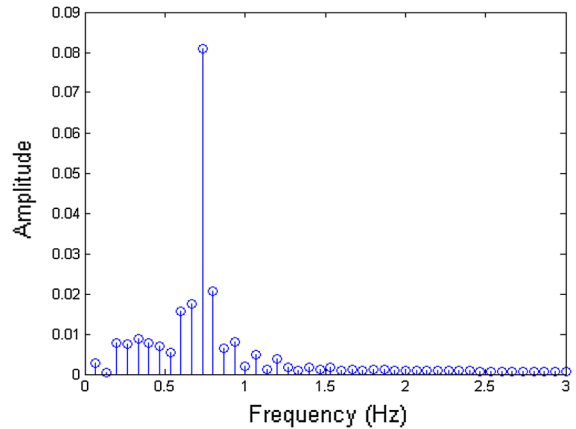


Fig. 52 Frequency spectrum of tangential swing with inverse dynamics control under continuous external disturbance

Table 3 Control schemes comparison

Control	Radial swing (rad)	Tangential swing (rad)
No control	0.31	0.18
No control with disturbances	0.59	0.4
Open-loop input shaper	0.14	0.07
Open-loop input shaper with disturbances	0.32	0.35
Closed-loop PID input shaper with disturbances	0.18	0.14
Inverse dynamics	0.07	0.03
Inverse dynamics with disturbances	0.13	0.12

5 Conclusion

The implementation and results of both the closed-loop PID input shaper and inverse dynamics have been presented. The control schemes have been tested on a marine crane model. The control schemes have been compared in terms of sway angle reduction. The open-loop input shaper has been effective in suppressing the oscillations, but it failed in suppressing the oscillations when there were any external disturbances. The closed-loop PID input shaper was effective in reducing the oscillations in the presence of external disturbances. The inverse dynamics controller showed better results and a higher oscillation reduction than the closed-loop PID input shaper (Table 3). On the other hand, the

results showed that all the control schemes increases the rise time of the system.

References

- Henry, R.J., Nayfeh, A.H.: Cargo pendulation reduction on ship-mounted cranes. MSc thesis. Virginia Polytechnic Institute and State University (1999)
- Karnopp, D.H., Fisher, F.E.: A strategy for moving mass from one point to another. *J. Frankl. Inst.* **329**, 881–892 (1992)
- Singer, N., Singhose, W., Kriikku, E.: An input shaping controller enabling cranes to move without sway, Ans 7th Topical Meeting on Robotics and Remote Systems (1997)
- Gurleyuk, S.S., Bahadir, O., Turkkan, Y., Usenti, H.: Improved three-step input shaping control of crane system. *WSEAS Trans. Syst.* **7**(6), 652–661 (2008)
- Teo, C.L., Ong, C.J., Xu, M.: Pulse input sequences for residual vibration reduction. *J. Sound Vib.* **211**(2), 157–177 (1998)
- Singhose, W., Seering, W., Singer, N.: Time-optimal negative input shapers. *J. Dyn. Syst. Meas. Control* **119**, 198–205 (1997)
- Singer, N.C., Seering, W.P.: Preshaping command inputs to reduce system vibration. *ASME J. Dyn. Syst. Meas. Control* (1988)
- Blackburn, D., Lawrence, J., Danielson, J., Singhose, W., Kamoi, T., Taura, A.: Radial-motion assisted command shapers for nonlinear tower crane rotational slewing. *Control Eng. Pract.* **18**, 523–531 (2010)
- Ahmad, M.A., Nasir, A.N.K., Ishak, H.: Techniques of anti-sway and input tracking control of a gantry crane system. In: Proceeding of the 2009 IEEE international conference on Mechatronics and automation (2009)
- Hurey, J.R.: The Intelligent Combination of Input Shaping and PID Feedback Control. Georgia Institute of Technology, Atlanta (2006)
- Ahmad, M.A., Mohamed, Z., Ismail, Z.H.: Hybrid input shaping and PID control of a flexible robot manipulator. *J. Inst. Eng.* **72**(3), 56–62 (2009)
- Fantoni, I., Lozano, R.: Non-Linear Control for Underactuated Mechanical Systems. Springer, London (2002)
- Zelei, A., Stépán, G.: Motion analysis of a crane as an underactuated robot, Gépészeti (2008)
- Hasan, M., Saha, M.C., Rahman, M.M., Sarker, R.I., Aditya, S.K.: Balancing of an inverted pendulum using PD controller. *Dhaka Univ. J. Sci.* **60**(1), 115–120 (2012)
- Avelar, C.A., Moreno-Valenzuela, J.: A feedback linearization controller for trajectory tracking of the Furuta pendulum. In: American Control Conference (ACC) (2014)
- Moreno-Valenzuela, J., Aguilar-Avelar, C., Puga-Guzmán, S.: Trajectory tracking control of the inertia wheel pendulum. In: 2nd International Conference on Control, Decision and Information Technologies (2014)
- Sorensen, K.L., Singhose, W., Dickerson, S.: Controller enabling precise positioning and sway reduction in bridge and gantry cranes. *Control Eng. Pract.* **15**, 825–837 (2007)
- Omar, H.M., Nayfeh, A.H.: Gain scheduling feedback control for the tower cranes. *J. Vib. Control* **9**, 399–418 (2003)
- Omar, H.M.: Control of gantry and tower cranes, Phd thesis, Virginia Polytechnic Institute and State University (2003)
- Wahyudi, J.J.: Design and implementation of a fuzzy logic controller for an intelligent gantry crane system. In: Proceedings of the 2nd International Conference on Mechatronics, pp. 345–351 (2005)
- Al-Mousa, A.A.: Control of rotary cranes using fuzzy logic and time-delayed feedback control, MSc thesis, Virginia Polytechnic Institute and State University (2000)
- Stewart, D.: A platform with six degrees-of-freedom. *Proc. Inst. Mech. Eng. Part 1*(180), 371–386 (1965)
- Abdel-Rahman, E.M., Nayfeh, A.H., Masoud, Z.N.: Dynamics and control of cranes: a review. *J. Vib. Control* **9**(7), 863–908 (2003)
- Lawrence, J.W.: Crane Oscillation Control: Nonlinear Elements and Educational Improvements. Georgia Institute of Technology, Atlanta (2006)
- Golafshani, AR.: Modeling and optimal control of tower crane motions, Phd thesis, University of Waterloo (1999)
- Devesse, W.: Slew control methods for tower cranes, MSc thesis, Stockholm, Sweden (2012)
- Masoud, Z.N., Nayfeh, A.H., Al-Mousa, A.: Delayed position feedback controller for the reduction of payload pendulations of rotary cranes. *J. Vib. Control* **9**(1–2), 257–277 (2003)
- Raubar, E., Vrancic, D.: Anti-sway system for ship-to-shore cranes. *J. Mech. Eng.* **58**, 338–344 (2012)
- Bazargan, Y., Zakeri, E., Ghahramani, A., Bazargan, K., Moezi, S.A.: Disturbance rejection control of 3-D overhead gantry crane system for regulation purpose. In: National Conference on Mechanical Engineering (2012)
- Matusko, J., Kolonic, F., Iles, S., Slutej, A.: Friction compensation of gantry crane model based on the B-spline neural compensator. In: 14th International Power Electronics and Motion Control Conference (2010)
- Dasgupta, B., Mruthyunjaya, T.S.: Closed-form dynamic equations of the general Stewart platform through the Newton–Euler approach. *Mech. Mach. Theory* **33**(7), 993–1012 (1998)
- Helinski, A.L.: Dynamic and kinematic study of a stewart platform using Newton–Euler techniques. U.S., Army Tank-Automotive Command (1990)
- Dasgupta, B., Mruthyunjaya, T.S.: A Newton–Euler formulation for the inverse dynamics of the Stewart platform. *Mech. Mach. Theory* **33**(8), 1135–1152 (1998)
- Singer, N.C.: Residual vibration reduction in computer controlled machines, Phd thesis. Massachusetts Institute of Technology (1989)
- Singhose, W., Seering, W., Singer, N.: Residual vibration reduction using vector diagrams to generate shaped inputs. *ASME J. Mech. Des.* **116**(2), 654–659 (1994)
- Blackburn, D., Singhose, W., Kitchen, J., Patrangenaru, V., Lawrence, J., Kamoi, T., Taura, A.: Advanced input shaping algorithm for nonlinear tower crane dynamics. In: Proceedings 8th International Conference, on Motion and Vibration Control. Daejeon, Korea (2006)
- Blackburn, D., Singhose, W., Kitchen, J., Patrangenaru, V., Lawrence, J., Kamoi, T., Taura, A.: Command shaping for nonlinear crane dynamics. *J. Vib. Control* **10**(0), 1–25 (2009)
- Mohamed, Z., Tokhi, M.O.: Vibration control of a single-link flexible manipulator using command shaping tech-

- niques. Proc. IMechE-I: J. Syst. Control Eng. **216**, 191–210 (2002)
39. Mailah, M., Yoong, C.S.: Disturbance rejection control applied to a gantry crane. Jurnal Mekanikal **25**, 64–79 (2008)
40. Tuan, L.A., Janchiv, A., Kim, G.-H., Lee, S.-G.: Feedback linearization control of overhead cranes with varying cable length. In: 11th International Conference on Control Automation and System (2011)
41. Yusop, A.M., Mohamed, Z., Sulaiman, N.A.: Inverse dynamic analysis with feedback control for vibration-free positioning of a gantry crane system. In: International Conference on Electronic Design (2008)
42. <https://dev.qu.tu-berlin.de/projects/sf-razor-9dof-ahrs/wiki/Tutorial>
43. <http://sine.ni.com/nips/cds/view/p/lang/en/nid/202802>